Supplemental Material

1.0 Heritage Algorithms

1.1 Dark Target

The DT algorithm was designed to retrieve spectral AOD from MODIS (Remer et al., 2005), has been adapted for VIIRS (Levy et al., 2015; Sawyer et al., 2020) and several geostationary sensors (Gupta et al., 2019; 2024). The algorithm is actually two algorithms, one for aerosols over ocean (Tanré et al., 1997) and one for aerosols over land (Kaufman et al., 1997; Levy et al. 2007ab). Before dividing into either the ocean or land algorithm paths, the mechanics of the retrieval begin with ingesting the satellite image and identifying those pixels inappropriate for an aerosol retrieval. Such pixels include suspended sediments and glint for the over ocean retrieval, bright terrestrial pixels such as deserts for the over land retrieval, and clouds, snow, ice for both ocean and land. These inappropriate pixels are masked from further attention. Then the algorithm organizes the image array into retrieval boxes of a specific size. For example, MODIS inputs of 0.5 km resolution pixels are organized into retrieval boxes of 20x20 pixels or nominally 10 km x 10 km. The measured spectral reflectance of all unmasked pixels within the retrieval box are averaged to produce the mean spectral reflectance that represents that box. The mean reflectance is corrected for gaseous absorption by water vapor, O_3, CO_2, N_2O, CH_4, O_2 and SO_2 (Patadia et al., 2018). These gas-corrected mean spectral reflectances will be the input for the actual retrieval (Levy et al. 2013).

The over ocean algorithm makes use of six wavelengths spanning the range of 0.55 µm to 2.25 µm (Tanré et al., 1997; Remer et al., 2005). A Look Up Table (LUT) is constructed of top-of-atmosphere spectral reflectances for ten single mode aerosol models, four representing particles in the fine mode and six in the coarse mode. Each aerosol model is defined by a single-mode size distribution and complex refractive index. All but one of the ten models assume spherical particles; one of the six coarse mode models is composed of a mixture of spheroids to represent nonspherical dust (Zhou et al., 2020ab). The LUT assumes a rough ocean surface with windspeed spanning from 2 m/s to 14 m/s (Cox and Munk, 1954) and water-leaving reflectance in the green wavelength (0.55 µm) of 0.005. All other wavelengths assume no water-leaving reflectance. The retrieval marches through the LUT, combining the top-of-atmosphere reflectance from one fine mode and one coarse mode using a mode-weighting factor to produce a combined top-of-atmosphere reflectance that can be compared with mean measured reflectance, wavelength by wavelength. The governing equation is,

$$\rho_\lambda^*(AOD) = \eta\rho_\lambda^{*f}(AOD) + (1-\eta)\rho_\lambda^{*c}(AOD) \quad (1)$$

Where $\rho^*_\lambda(AOD)$ represents the LUT top-of-atmosphere reflectance at wavelength, λ, for a particular AOD in the LUT, the f and c superscripts represent the fine mode and coarse mode, respectively and η is the mode weighting factor. Reflectance without an f or c superscript represents the total reflectance that should compare with the satellite measurement. The average difference between measured reflectance and LUT reflectance is minimized in a least squares sense across all six wavelengths to find the combination of modes and the aerosol loading of each one that best represents the spectral reflectance at the top of atmosphere. The result of the retrieval is an AOD, the two chosen modes and the mode weighting parameter, η.

The DT over land algorithm makes use of three wavelengths, one in the blue, one in the red and one in the 2 μm range (Levy et al., 2007ab). The land LUT is constructed using four bimodal aerosol models, three are dominated by the fine mode but differ in absorption properties and one is dominated by the coarse mode. The three fine mode-dominated models consist of spherical particles and are fixed by seasonal global maps. The coarse mode-dominated model consists of a mix of spheroids and is global. The greatest challenge in retrievals over land is in constraining the surface. The DT land algorithm uses empirical relationships between blue, red and 2 μm surface reflectance, modified by scattering angle and a measure of surface "greenness". During the retrieval, the LUT's Rayleigh scattering component is modified for elevation of the target. Differences between top-of-atmosphere reflectances are minimized in the blue and red wavelengths to obtain AOD and the relative weighting of fine-dominated and coarse-dominated bimodal models that define the spectral dependence of the AOD in the visible, from blue through red.

The contribution of the DT algorithm to UAA is to produce six wavelengths of AOD from 0.55 μm to 2.25 μm over ocean along with a size distribution model consisting of one fine mode and one coarse mode and the relative weighting between them (η). Over land when surface reflectance is sufficiently dark, the DT algorithm produces AOD in three visible channels, with the other parameters considered to be diagnostics.

1.2 Deep Blue

The Deep Blue (DB) algorithm was originally developed to retrieve aerosol properties over bright surfaces, such as deserts and barren areas, thereby enhancing the spatial coverage of aerosol product (Hsu et al., 2004, 2006). This was achieved by primarily utilizing blue wavelengths (0.41-0.49 μm), at which the contribution of surface reflectance to the top-of-atmosphere signal is significantly lower compared to longer wavelengths, thus providing better retrieval sensitivity. Like the DT algorithm, the primary DB product is spectral AOD, with secondary parameters including Ångstrom exponent and aerosol type.

Since its conception, the DB algorithm has been extended to near-global land surfaces (excluding cloud, snow, or ice-covered areas) by adopting a DT-like approach for dark surfaces (Hsu et al., 2013), and to water surfaces through the development of the Satellite Ocean Aerosol Retrieval (SOAR) algorithm (Sayer et al., 2012, 2018). The algorithm suite has been successfully applied to several sensors, including the Advanced Very High Resolution Radiometer (AVHRR; Hsu et al, 2017; Sayer et al., 2017), the Sea-viewing Wide Field-of-view Sensor (SeaWiFS; Hsu et al., 2013), MODIS (Hsu et al., 2013), and VIIRS (Hsu et al., 2019; Lee et al., 2024), as well as multiple geostationary sensors, enabling the creation of a consistent, long-term aerosol climate data record.

The DB over-land algorithm uses three different approaches for determining surface reflectance, depending on surface characteristics. First, surface reflectance over bright surfaces, defined as the normalized difference vegetation index (NDVI; Tucker, 1979) less than 0.1, is determined using a minimum reflectance technique. Several years of Rayleigh- and gas-corrected top-of-atmosphere reflectance data, aggregated into 0.1° grids, are used to derive the minimum reflectance in each grid as a function of scattering angle and season. Second, over dark surfaces (NDVI 0.1), surface reflectance is estimated using interspectral relationships between visible bands (0.49 and 0.67 µm) and SWIR band (~2 µm). Third, over areas where these two approaches show limitations (often bright, heterogeneous areas such as urban or croplands), a hybrid approach is employed. This method combines a predefined bidirectional reflectance distribution function (BRDF) derived at AERONET sites within the target domain with the minimum reflectance database at a fixed scattering angle (135°). The primary wavelengths used for aerosol retrievals are 0.41 and 0.49 µm over bright surfaces and in the hybrid approach, and 0.49 and 0.67 µm over dark surfaces.

The DB algorithm uses two aerosol optical model sets, one for fine-dominated aerosols and one for mineral dust. A bimodal lognormal size distribution is assumed, with fine-mode AOD fractions of 0.90 and 0.15, respectively, and SSA ranging from 0.89-0.995. The fine-dominated model assumes spherical particles, while the dust model assumes spheroids (Lee et al., 2017). In the retrieval process, SSA is predefined by geographic region, season, and AOD to better represent changing aerosol characteristics.

The UAA algorithm is based on the VIIRS DB Version 1 algorithm without incorporating the SOAR algorithm, relying solely on DT algorithm for ocean retrievals. Although PACE OCI lacks IR channels, which introduces limitations in detecting smoke and dust, it provides reliable AOD retrieval over land using three visible channels with which DB performs optimally.

1.3 Near-UV (NUV)

The near-UV (NUV) spectral region offers unique sensitivity of TOA observations to aerosol extinction and absorption, along with relatively lower land surface albedo over continental dark and desert surfaces. The UV Aerosol Index (UVAI), first defined as a residue parameter in the total column Ozone retrieval from the Nimbus-7/TOMS instrument (Herman et al., 1997), has been proven as an excellent, semi-quantitative parameter to identify the presence of UV-light-absorbing aerosols, such as carbonaceous aerosols in smoke plumes and mineral dust, in the atmospheric column over the oceans and the continents and above bright reflecting backgrounds such as clouds, sea-ice, and snow-covered surfaces. Quantitatively, the residue represents the spectral contrast in the signal between the two NUV wavelengths after the removal of Rayleigh scattering effects following the Lambertian Equivalent Reflectivity (LER) approach adopted in the early 1990s. Since most of the signal in this residue parameter is attributed to the aerosol effects, it was termed as UVAI and formulated as,

$$UVAI = -100 \left[\log\left(\frac{I_{sm}}{I_{lm}}\right) meas - \log\left(\frac{I_{sc}}{I_{lc}}\right) calc\right] \quad \text{(S1)}$$

Where, I_{sm} and I_{lm} are the measured TOA radiances at a shorter and longer wavelength, respectively, from the satellite sensor and Isc and Ilc are the calculated radiance following the LER approach with the longer wavelength as a reference. The UVAI varies between slightly negative numbers, down to about -1, generally associated with small size non-absorbing aerosol types, around zero for most clouds, and positive values for UV-absorbing aerosol types. The UVAI magnitude in the presence of absorbing aerosols depends mainly on the aerosol optical depth (AOD), and the height of the absorbing aerosol layer (Torres et al., 1998). Double-digit UVAI values are typically observed in the aftermath of pyro-Cb events (Fromm et al, 2010) when optically thick carbonaceous aerosol layers reach the upper troposphere and stratosphere, as documented in the aftermath of the 2017 British Columbia pyroCb event (Torres et al., 2020a). Although most of the positive signal in UVAI is known to be caused by the presence of absorbing aerosols, UVAI-like signal can be generated by surface types with spectrally varying optical properties such as deserts, and the remote ocean surfaces where pure water UV absorption effects (Lee et al., 2015) generate positive UVAI values (up to about 1). To account for the effects of these surfaces, a first order, empirical correction was introduced that subtracts surface LER, based on the long-term monthly climatology values, from the calculated LER before deriving UVAI. In recent years, further refinements to the UVAI have been made to account for the angular scattering effects of water clouds. Large negative values of UVAI over seasonally occurring cloudy skies, such as southern Africa and the southeastern Atlantic Ocean, necessitated this refinement. The new formulation of UVAI and its regional and global application are described in Torres et al., (2018).

By leveraging the strong sensitivity to aerosols, coupled with lower surface albedo, a two-channel NUV algorithm was developed and applied to the TOMS sensor aboard Nimbus-7 and EarthProbe platforms to deduce for the first time the global distribution of UV-absorbing aerosols over the oceans and the continents (Torres et al., 2002). Radiative transfer simulations revealed that the TOA observations between the 340-380 nm spectral region are primarily sensitive to the three aerosol parameters: AOD, SSA, and aerosol layer height (ALH). The dependence of the NUV radiances to ALH stems from the radiative interactions between aerosols and molecular scattering. For instance, elevated layers of aerosols increase the likelihood of enhanced aerosol absorption caused by Rayleigh scattering beneath these aerosols. When constrained with an aerosol model and assumed ALH, the NUV algorithm retrieves AOD and SSA simultaneously at longer wavelength (either at 380 nm or 388 nm, depending on the sensor). Subsequently, an improved version of the algorithm was also designed and applied to the long-term observation record of the Ozone Monitoring Instrument (OMI) (Torres et al., 2007, Jethva and Torres, 2011; Torres et al., 2018). The NUV aerosol record has been further extended with observations from the DSCOVR-EPIC (Ahn et al., 2021), and more recently from the Sp5-TROPOMI (Torres et al., 2020b). This long-term data continuity project has delivered nearly 40 years of a global product of aerosol extinction (AOD) and absorption (SSA).

OCI's hyperspectral capability allows continuation of NUV aerosol retrievals at much higher spatial resolution than its predecessor sensors with UV observations described above. The strength and unique philosophy of the UAA further advances the NUV retrieval capability by providing a constraint on the total aerosol loading (AOD) first retrieved at the visible wavelengths, followed by its conversion to the UV wavelengths (354 nm and 388 nm). As noted previously, the TOA signal at the two NUV wavelengths exhibited a marked sensitivity to AOD, SSA, and ALH, which is further illustrated in Figure S1 below. The theoretical RT simulations are shown for a fine mode dominated carbonaceous aerosol model for varying imaginary part of the refractive index or SSA and ALH at two distinct AODs. The grey lines (blue lines) connect simulations for varying ALH values (SSA values) at a fixed value of SSA (ALH). This sensitivity of TOA radiances and their color ratio, when constrained with columnar AOD, forms the physical basis for simultaneously retrieving the SSA/ALH pair from OCI observations. Such an approach was first demonstrated in Satheesh et al. (2009) employing MODIS-retrieved AOD to constrain the OMI retrieval, freeing OMI from making an a priori assumption of ALH and allowing rather a more direct retrieval of aerosol absorption and ALH. The extrapolation of MODIS AODs from visible to NUV wavelength relied on the spectral dependence of the MODIS-retrieved visible and NUV spectral AODs. The suggested approach by Satheesh et al. (2009) was successfully demonstrated over the tropical Atlantic and Arabian Sea oceanic regions.

The OCI, owing to its spatiotemporally consistent UV to near-IR hyperspectral observational capability, presents a perfect opportunity to employ such an approach on a daily global basis. UAA aims to demonstrate the synergy of NUV and visible-NIR observations of OCI to derive a comprehensive suite of aerosol products that was either very limited or non-existent in the past.

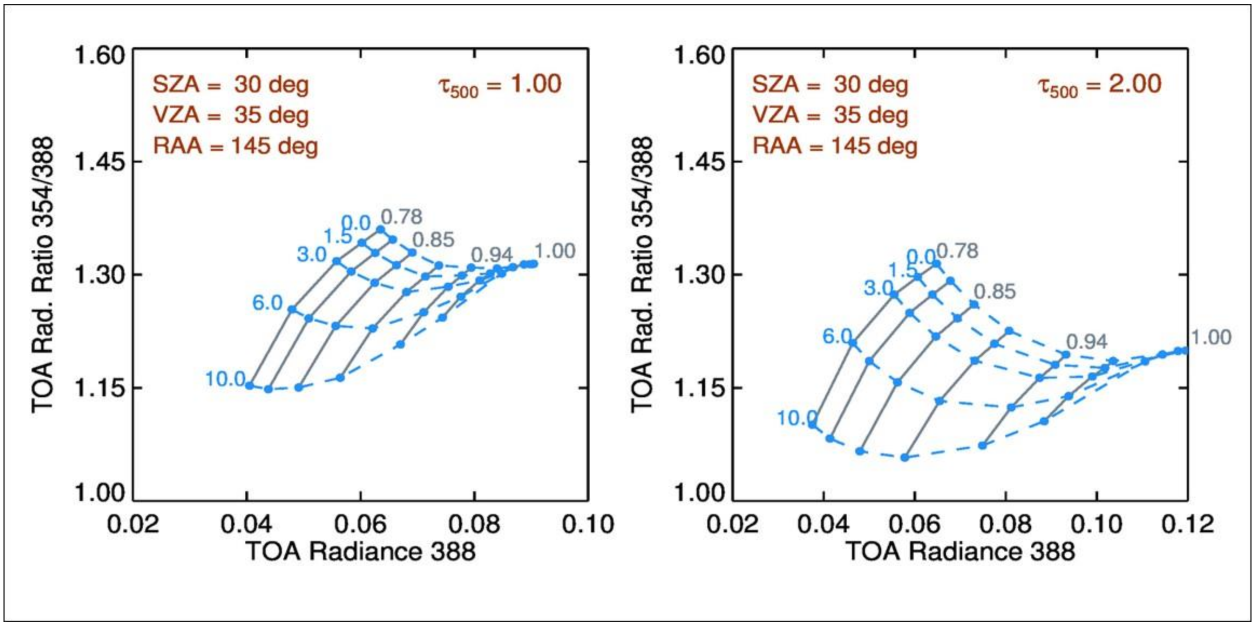

Figure S1 Radiative transfer calculations of TOA radiances and color ratio at NUV wavelengths of 354 nm and 388 nm of an assumed carbonaceous aerosol model. The results are shown for two distinct AODs (500 nm) of 1.0 (left) and 2.0 (right). Grey lines (blue lines) connect simulations for varying ALH values (SSA values) at a fixed value of SSA (ALH).

2.0 Extrapolation of AOD to UV using Machine Learning

Figures S2 and S3 demonstrate the ML model over selected dust and smoke scenes. Figure S2 shows model predicted 0.34 µm AOD using DT VIIRS AOD over the west coast of North America during a wildfire event on 2018 November 10th, with point values of AERONET AOD overlayed onto the image. Smoke flows out over the ocean from fire sources on land. Over land, the predicted AOD are mostly in line with what AERONET measured for both wavelengths despite the large variation of AOD observed in the image. Similarly, Figure S3 shows a dust case in the Caribbean on 2020 June 22nd, although there is very limited over land in the image, the predicted AOD at island sites is very close to AERONET values on the east side of the image at the Rugged Point station on Barbados. The predicted values at other island sites in the image capture the same regional gradient as do the AERONET stations, but run a bit higher than the actual measurements.

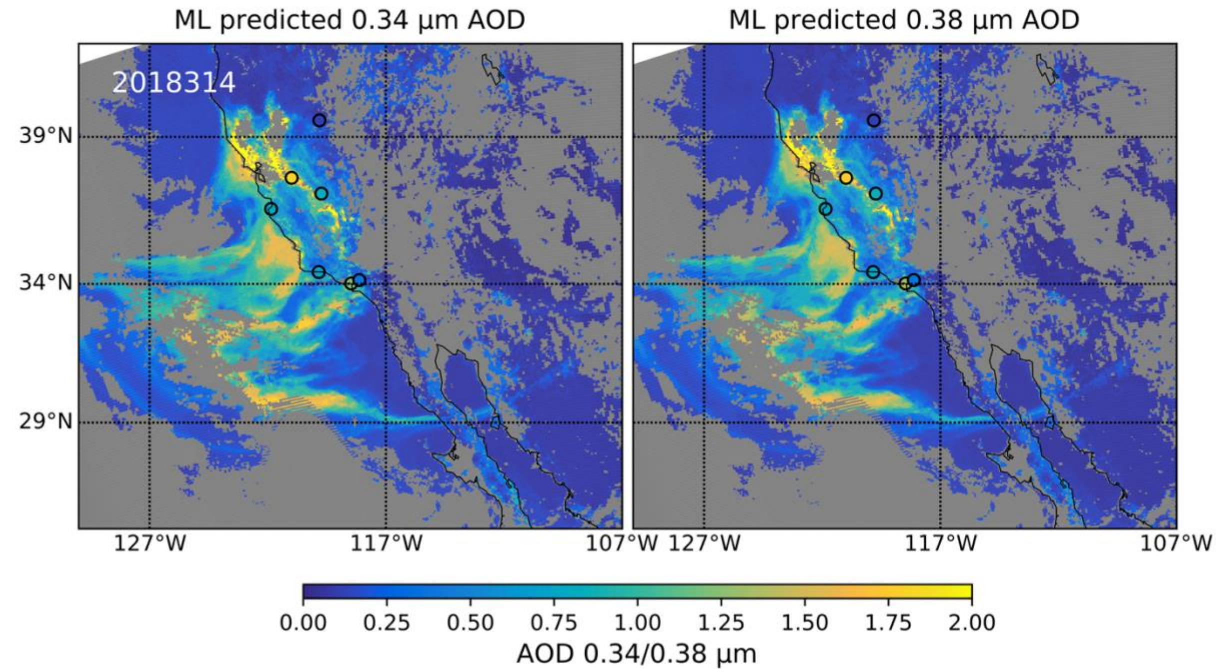

Figure S2. ML predicted AOD at UV wavelengths, 0.34 µm (left) and 0.38 µm (right), using VIIRS DT AOD retrievals in three visible wavelengths. AERONET point measurements of AOD at the same UV wavelengths is shown as an overlay of colored circles at the station locations. The event is a smoke case on the west coast of the United States on November 10th 2018.

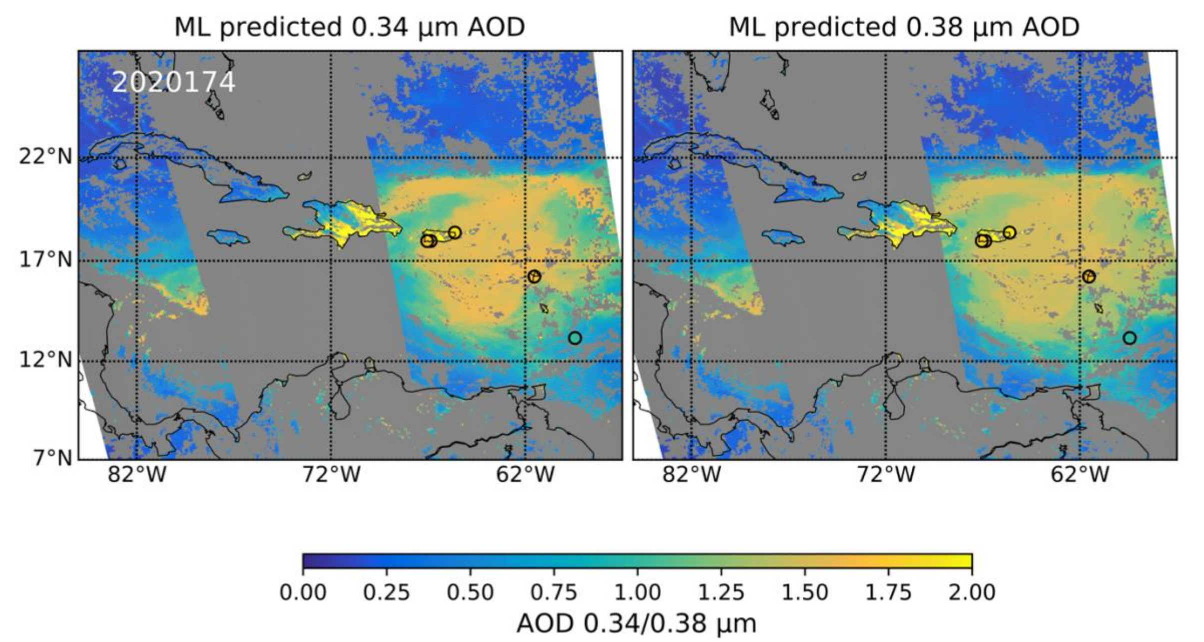

Figure S3. Same as Figure S2 but for a dust case over the eastern Caribbean on June 22nd 2020.

The summary and comparison of the uncertainties associated with extrapolation of AOD into the UV is shown in Tables S1 and S2 where the percentage of extrapolations falling within a succession of relative and absolute error bars are shown. In all cases the Machine Learning extrapolation surpasses even the quadratic one, achieving one standard deviation of extrapolations falling within ±0.15 relative and ±20% absolute error bars for 0.38 μm and ±0.20 relative and ±20% absolute error bars for 0.34 μm for our test situation at the Alta Floresta AERONET station. Graphically we see the advantages of the ML model over the other extrapolations in Figure 3 of the main text where the gray line for the ML regression fit overlaps the black 1:1 line so well that it is invisible in the figure.

Table S1. Fraction of extrapolations falling within specified relative error bars (top) or absolute error bars (bottom) using different extrapolation methods: Machine Learning, Quadratic Fit and linear 2-wavelength Angstrom Exponent fit using either 0.675 μm and 0.44 μm or 0.50 μm and 0.44 μm wavelengths. Results based on extrapolation of AERONET Alta Floresta aerosol optical depth (AOD) measurements in the visible to the UV wavelength of 0.38 μm and compared to AERONET measured AOD at that UV wavelength. 127 extrapolations performed and analyzed

Relative Error	**±5%**	**±10%**	**±15%**	**±20%**	**±25%**
Machine Learning	0.29	0.50	0.59	0.72	0.77
Quadratic	0.20	0.41	0.54	0.62	0.72
AngExp 675/440	0.09	0.16	0.28	0.36	0.47
AngExp 500/440	0.06	0.13	0.32	0.37	0.45
Absolute Error	**±0.05**	**+0.10**	**±0.15**	**±0.20**	**±0.25**
Machine Learning	0.27	0.54	0.69	0.80	0.86
Quadratic	0.19	0.37	0.56	0.69	0.75
AngExp 675/440	0.19	0.25	0.40	0.54	0.68
AngExp 500/440	0.13	0.22	0.41	0.52	0.65

Table S2. Same as Table S1 but for the 0.34 μm wavelength and 146 extrapolations analyzed.

Relative Error	**±5%**	**±10%**	**±15%**	**±20%**	**±25%**

Machine Learning	0.21	0.47	0.60	0.73	0.80
Quadratic	0.14	0.30	0.48	0.64	0.72
AngExp 675/440	0.03	0.14	0.21	0.29	0.38
AngExp 500/440	0.07	0.14	0.18	0.25	0.32
Absolute Error	**±0.05**	**+0.10**	**±0.15**	**±0.20**	**±0.25**
Machine Learning	0.23	0.42	0.60	0.68	0.79
Quadratic	0.14	0.29	0.45	0.58	0.66
AngExp 675/440	0.07	0.16	0.30	0.44	0.49
AngExp 500/440	0.09	0.17	0.25	0.36	0.49

3.0 Retrieval of SSA over ocean using the DT approach

To accomplish the DT retrieval in the UV, the DT LUT is extended for two new wavelengths at 0.354 µm and 0.388 µm. Using the previously defined size parameters from the heritage LUT, each of the original ten modes is expanded into four different models by varying the imaginary part of the refractive index for each of the two UV wavelengths. The real part of the refractive index is kept the same value from the heritage blue wavelength. Table S3 shows the values of complex refractive index for each UV wavelength, the geometric mean (r_g), geometric standard deviation (σ) and effective radius (r_{eff}) of the lognormal size distribution. Models 1 – 9 are assumed spherical with their LUT calculations performed using Mie code (Remer et al., 2005), while Model 10 is nonspherical and reserved for dust retrievals (Zhou et al., 2020). The LUT calculations in the two new UV channels are done for each of the four imaginary indices, at four different aerosol layer heights and at four surface wind speeds. The values of the four aerosol layer heights are 1.5, 3.0, 6.0, 10.0 km,. The four windspeeds are 2, 6, 10, 14 m/s.

Table S3. Expanded Look Up Table for Dark Target retrieval over ocean that allows for a range of absorption properties for each of the 10 traditional non-absorbing aerosol models. Models 1 – 9 are spherical. Model 10 is non-spherical.

Fine Particles

	0.354 µm	0.388 µm	r_g	σ	r_{eff}
1	A: 1.45-0.0035i B: 1.45-0.0078i	A: 1.45-0.0035i B: 1.45-0.0075i	0.07	0.40	0.10

	C: 1.45-0.00607i D: 1.45-0.0211i	C: 1.45-0.00515i D: 1.45-0.0161i			
2	A: 1.45-0.0035i B: 1.45-0.0078i C: 1.45-0.00663i D: 1.45-0.0230i	A: 1.45-0.0035i B: 1.45-0.0075i C: 1.45-0.00619i D: 1.45-0.0193i	0.06	0.60	0.15
3	A: 1.40-0.0020i B: 1.40-0.0078i C: 1.40-0.00386i D: 1.40-0.0134i	A: 1.40-0.0020i B: 1.40-0.0075i C: 1.40-0.00391i D: 1.40-0.0122i	0.08	0.60	0.20
4	A: 1.40-0.0020i B: 1.40-0.0078i C: 1.40-0.00234i D: 1.40-0.00814i	A: 1.40-0.0020i B: 1.40-0.0075i C: 1.40-0.00236i D: 1.40-0.00736i	0.10	0.60	0.25

Coarse Particles

	0.354 μm	0.388 μm	r_g	σ	r_{eff}
5	A: 1.35-0.001i B: 1.35-0.0065i C: 1.35-0.00259i D: 1.35-0.009i	A: 1.35-0.001i B: 1.35-0.0056i C: 1.35-0.00237i D: 1.35-0.00739i	0.40	0.60	0.98
6	A: 1.35-0.001i B: 1.35-0.0065i C: 1.35-0.00289i D: 1.35-0.0101i	A: 1.35-0.001i B: 1.35-0.0056i C: 1.35-0.00267i D: 1.35-0.00832i	0.60	0.60	1.48
7	A: 1.35-0.001i B: 1.35-0.0065i C: 1.35-0.00332i D: 1.35-0.01161i	A: 1.35-0.001i B: 1.35-0.0056i C: 1.35-0.00296i D: 1.35-0.00923i	0.80	0.60	1.98
8	A: 1.53-0.000i B: 1.53-0.0065i C: 1.53-0.00164i D: 1.53-0.009i	A: 1.53-0.000i B: 1.53-0.0056i C: 1.53-0.00150i D: 1.53-0.010i	0.60	0.60	1.48
9	A: 1.53-0.000i B: 1.53-0.0065i C: 1.53-0.00114i D: 1.53-0.011i	A: 1.53-0.000i B: 1.53-0.0056i C: 1.53-0.00101i D: 1.53-0.010i	0.50	0.80	2.50
10	A: 1.53-0.0040i B: 1.53-0.0071i C: 1.53-0.0102i D: 1.53-0.0132i	A: 1.53-0.0032i B: 1.53-0.0063i C: 1.53-0.0094i D: 1.53-0.0102i	0.5	0.6	1.23

The DT UAA retrieval over ocean begins the same as the heritage DT algorithm. It uses the VIS to SWIR bands to retrieve AOD at 0.55 μm, one fine mode, one coarse mode and η from Eq. S1. The surface windspeed is needed for the VIS-SWIR retrieval and is provided by ancillary data. The retrieved size distribution defines a unique spectral dependence for AOD, allowing for extrapolation of the AOD across the spectrum including to the two UV wavelengths. The extrapolation does not make use of the Angstrom Exponent and can curve in log-log space (Eck et al., 1999). The retrieved bimodal size distribution limits the choice of spectral absorption in the UV to one of four possibilities (A, B, C or D) in Table 1. These models represent a dynamic range of UV aerosol absorption characteristics taken from measurements and appearing in the literature. The models cover a range of aerosol types from desert dust to carbonaceous aerosol types (Krotkov et al. 2005; Dinar et al., 2007; Mogo et al., 2012; Wagner et al., 2012; Rocha Lima et al., 2014, 2018). Note that the fine and coarse mode imaginary part of the refractive index of any of the four possible models are linked but not the same. This leaves only two free parameters remaining, the UV spectral absorption model (A, B, C or D), plus the aerosol layer height. The retrieval minimizes the difference between the measured and LUT values of reflectances in the two UV wavelengths for each of the four aerosol layers, then minimizes again to find the layer with the smallest error. This provides a value of SSA at 0.354 µm and 0.388 µm.

The SSA is extrapolated to 0.55 µm using a multiple regression model parameterized on the Angstrom Exponent for AOD and the difference between SSA at 0.388 µm and 0.354 µm. The parameterization is based on the data base presented as Table 3 in Kayetha et al. (2022). The dependency on Angstrom Exponent distinguishes between dust-like aerosol and carbonaceous aerosol of Kayetha et al. (2022) and the spectral dependence on SSA in the UV further refines the projection into the visible. The result of the UAA DT retrieval over ocean are the AOD from 0.354 µm to 2.25 µm in 9 wavelengths, the η parameter that is an indication of aerosol fine mode fraction and SSA at 0.354 µm, 0.388 µm and 0.55 µm. The aerosol layer height is also reported but is considered a diagnostic of the retrieval and not a validated physical parameter.

4.0 Comparison of OCI and TropOMI UVAI

One of the UAA innovations is the production of UVAI at native sensor resolution, 1.1 km. Here we compare the UAA product derived from OCI measurements with the more experienced TropOMI product produced at 3.5x5 km. The products from the two sensors represent the same region on the same day. The qualitative and quantitative similarities between the UVAI from the two sensors are strong. This builds confidence in the OCI UVAI product and in the calibration of the OCI UV wavelengths.

The advantages of the 1.1 km product are not obvious in this comparison. Any advantage of a finer resolution UVAI product would be realized on the local scale, not the continental scales shown here. We leave analysis at the local scale for future research.

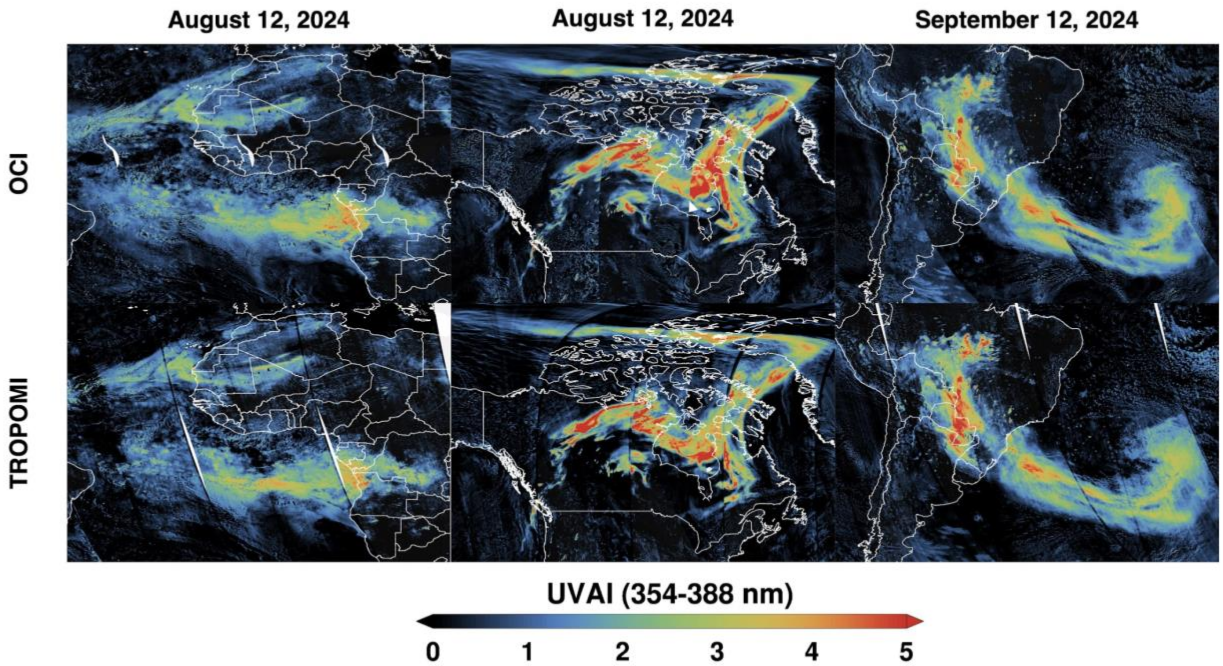

Figure S4. Regional maps of UVAI (0.354-0.388 µm) derived from OCI observations at a native spatial resolution of ~1.1 km (top) and from TropOMI resolution at 3.5x5 km for Aug 12 (left and center) and Sep 12 (right), 2024. Locations from left to right are: Africa with the Atlantic Ocean, Canada, and South America with the Atlantic Ocean.

5.0 References

Ahn, C., Torres, O., Jethva, H., Tiruchirapalli, R., and Huang, L.-K.: Evaluation of aerosol properties observed by DSCOVR/EPIC instrument from the Earth-Sun Lagrange 1 Orbit. *J. Geophysi. Res. Atmos.*126, e2020JD033651, https://doi.org/10.1029/2020JD033651, 2021.

Cox, C., and Munk, W.: Statistics of the sea surface derived from sun glitter, *J. Mar. Res.*, 13, 198–208, 1954.

Dinar, E., Riziq, A. A., Spindler, C., Erlick, C., Kiss, G., and Rudich, Y.: The complex refractive index of atmospheric and model humic-like substances (HULIS) retrieved by a cavity ring down aerosol spectrometer (CRD-AS), Faraday Discuss., 137, 279-295, doi: https://doi.org/10.1039/B703111D, 2007.

Eck, T. F., Holben, B. N., Reid, J. S., Dubovik, O., Smirnov, A., O'Neill, N. T., Slutsker, I., and Kinne, S.: Wavelength dependence of the optical depth of biomass burning, urban, and desert dust aerosols, J. Geophys. Res., 104(D24), 31333–31349, doi: https://doi.org/10.1029/1999JD900923, 1999.

Fromm, M., Lindsey, D.T., Servranckx, R., Yue, G., Trickl, T., Sica, R., Doucet, P. and Godin-Beekmann, S.: The Untold Story of Pyrocumulonimbus. *Bull. Amer. Meteor. Soc.*, **91**, 1193–1210, https://doi.org/10.1175/2010BAMS3004.1, 2010.

Gupta, P., Levy, R. C., Mattoo, S., Remer, L. A., Holz, R. E., and Heidinger, A. K.: Applying the Dark Target aerosol algorithm with Advanced Himawari Imager observations during the KORUS-AQ field campaign, Atmos. Meas. Tech., 12, 6557–6577, doi: https://doi.org/10.5194/amt-12-6557-2019, 2019.

Gupta, P., Levy, R. C., Mattoo, S., Remer, L. A., Zhang, Z., Sawyer, V., Wei, J., Zhao, S., Oo, M., Kiliyanpilakkil, V. P., and Pan, X.: Increasing aerosol optical depth spatial and temporal availability by merging datasets from geostationary and sun-synchronous satellites, Atmos. Meas. Tech., 17, 5455–5476, https://doi.org/10.5194/amt-17-5455-2024, 2024.

Herman, J. R., Bhartia, P. K., Torres, O., Hsu, C., Seftor, C., and Celarier, E.: Global distribution of UV-absorbing aerosols from Nimbus 7/TOMS data, J. Geophys. Res., 102(D14), 16911–16922, doi: https://doi.org/10.1029/96JD03680, 1997.

Hsu, N. C., Tsay, S. C., King, M. D., & Herman, J. R.: Aerosol properties over bright-reflecting source regions. IEEE Transactions on Geoscience and Remote Sensing, 42(3), 557–569. doi.org/10.1109/TGRS.2004.824067, 2004.

Hsu, N. C., Tsay, S.-C., King, M. D., & Herman, J. R.: Deep blue retrievals of Asian aerosol properties during ACE-Asia. IEEETransactions on Geoscience and Remote Sensing, 44(11), 3180–3195. doi.org/10.1109/TGRS.2006.879540, 2006.

Hsu, N. C., Jeong, M.-J., Bettenhausen, C., Sayer, A.M., Hansell, R., Seftor, C. S., Huang, J., and Tsay, S.-C.: Enhanced Deep Blue aerosol retrieval algorithm: The second generation, *J. Geophys. Res. Atmos.*, 118, 9296–9315, doi:10.1002/jgrd.50712, 2013.

Hsu, N. C., Lee, J., Sayer, A. M., Carletta, N., Chen, S.-H., Tucker, C. J., Holben, B. N., and Tsay, S.-C.: Retrieving near-global aerosol loading over land and ocean from AVHRR, J. Geophys. Res. Atmos., 122, doi:10.1002/2017JD026932, 2017.

Hsu, N. C., Lee, J., Sayer, A. M., Kim, W., Bettenhausen, C., & Tsay, S.-C.: VIIRS Deep Blue aerosol products over land: Extending the EOS long-term aerosol data records. *Journal of Geophysical Research: Atmospheres*, **124**(7), 4026–4053. doi.org/10.1029/2018JD029688, 2019.

Jethva, H. and Torres, O.: Satellite-based evidence of wavelength-dependent aerosol absorption in biomass burning smoke inferred from Ozone Monitoring Instrument, Atmos. Chem. Phys., 11, 10541–10551, doi: https://doi.org/10.5194/acp-11-10541-2011, 2011.

Kaufman, Y. J., Tanré, D., Remer, L. A., Vermote, E., Chu, A., and Holben, B. N.: Operational remote sensing of tropospheric aerosol over land from EOS moderate resolution imaging spectroradiometer, J. Geophys. Res., 102, 17051-17067, doi: https://doi.org/10.1029/96JD03988, 1997.

Kayetha, V., Torres, O., and Jethva, H.: Retrieval of UV–visible aerosol absorption using AERONET and OMI–MODIS synergy: spatial and temporal variability across major aerosol environments, Atmos. Meas. Tech., 15, 845–877, https://doi.org/10.5194/amt-15-845-2022, 2022.

Krotkov, N., Bhartia, P. K., Herman, J., Slusser, J., Scott, G., Labow, G., Vasilkov, A. P., Eck, T. F., Dubovik, O., and Holben, B. N.: Aerosol ultraviolet absorption experiment (2002 to 2004), part 2: Absorption optical thickness, refractive index, and single scattering albedo, Opt. Eng., 44(4), 1–17, doi.org/10.1117/1.1886819, 2005.

Lee, J., Hsu, N. C., Sayer, A. M., Bettenhausen, C., and Yang, P.: AERONET-based nonspherical dust optical models and effects on the VIIRS Deep Blue/SOAR over water aerosol product, J. Geophys. Res. Atmos., 122, 10,384–10,401, doi.org/10.1002/2017JD027258, 2017.

Lee, J., Hsu, N. C., Kim, W. V., Sayer, A. M., & Tsay, S. C.: VIIRS version 2 deep blue aerosol products. J. Geophys. Res. Atmos., 129(6), /doi:10.10292023JD040082, 2024.

Lee, Z., Wei, J., Voss, K., Lewis, M., Bricaud, A. and Huot, Y.: Hyperspectral absorption coefficient of “pure” seawater in the range of 350–550 nm inverted from remote sensing reflectance. Appl. Opt. 54, 546-558, https://opg.optica.org/ao/abstract.cfm?URI=ao-54-3-546 2015.

Levy, R. C., Remer, L. A., and Dubovik, O.: Global aerosol optical properties and application to Moderate Resolution Imaging Spectroradiometer aerosol retrieval over land, J. Geophys. Res., 112, D13210, doi: https://doi.org/10.1029/2006JD007815, 2007a.

Levy, R. C., Remer, L., Mattoo, S., Vermote, E., and Kaufman, Y. J.: Second-generation operational algorithm: Retrieval of aerosol properties over land from inversion of Moderate Resolution Imaging Spectroradiometer spectral reflectance, J. Geophys. Res., 112, D13211, doi: https://doi.org/10.1029/2006JD007811, 2007b.

Levy, R. C., Mattoo, S., Munchak, L. A., Remer, L. A., Sayer, A. M., Patadia, F., and Hsu, N. C.: The Collection 6 MODIS aerosol products over land and ocean, Atmos. Meas. Tech., 6, 2989–3034, doi: https://doi.org/10.5194/amt-6-2989-2013, 2013.

Levy, R. C., Munchak, L. A., Mattoo, S., Patadia, F., Remer, L. A., and Holz, R. E.: Towards a long-term global aerosol optical depth record: applying a consistent aerosol retrieval algorithm to MODIS and VIIRS-observed reflectance, Atmos. Meas. Tech., 8, 4083–4110, doi: https://doi.org/10.5194/amt-8-4083-2015, 2015.

Mogo, S., Cachorro, V. E., and de Frutos, A. M.: In situ UV-VIS-NIR absorbing properties of atmospheric aerosol particles: Estimates of the imaginary refractive index and comparison with columnar values, Journal of Environmental Management, 111, 267-271, doi: https://doi.org/10.1016/j.jenvman.2012.07.027, 2012.

Patadia, F., Levy, R. C., and Mattoo, S.: Correcting for trace gas absorption when retrieving aerosol optical depth from satellite observations of reflected shortwave radiation, Atmos. Meas. Tech., 11, 3205–3219, https://doi.org/10.5194/amt-11-3205-2018, 2018.

Remer, L. A., Kaufman, Y. J., Tanré, D., Mattoo, S., Chu, D. A., Martins, J. V., Li, R.-R., Ichoku, C., Levy, R. C., Kleidman, R. G., Eck, T. F., Vermote, E., and Holben, B. N.: The MODIS aerosol algorithm, products and validation. J. Atmos. Sci., 62, 947-973, doi: https://doi.org/10.1175/JAS3385.1, 2005.

Rocha-Lima, A., Martins, J. V., Remer, L. A., Krotkov, N. A., Tabacniks, M. H., Ben-Ami, Y., and Artaxo, P.: Optical, microphysical and compositional properties of the Eyjafjallajökull volcanic ash, Atmos. Chem. Phys., 14, 10649–10661, doi: https://doi.org/10.5194/acp-14-10649-2014, 2014.

Rocha-Lima, A., Martins, J. V., Remer, L. A., Todd, M., Marsham, J. H., Engelstaedter, S., Ryder, C. L., Cavazos-Guerra, C., Artaxo, P., Colarco, P., and Washington, R.: A detailed characterization of the Saharan dust collected during the Fennec campaign in 2011: in situ ground-based and laboratory measurements, Atmos. Chem. Phys., 18, 1023–1043, doi: https://doi.org/10.5194/acp-18-1023-2018, 2018.

Satheesh, S. K., Torres, O., Remer, L. A., Babu, S. S., Vinoj, V., Eck, T. F., Kleidman, R. G., and Holben, B. N.: Improved assessment of aerosol absorption using OMI-MODIS joint retrieval, J. Geophys. Res., 114, D05209, doi: https://doi.org/10.1029/2008JD011024, 2009.

Sawyer, V., Levy, R., Mattoo, S., Cureton, G. Shi, Y. Remer, L.A.: Continuing the MODIS Dark Target aerosol time series with VIIRS, Remote Sens. 12, 308, doi: https://doi.org/10.3390/rs12020308, 2020.

Sayer, A. M., Hsu, N. C., Bettenhausen, C., Ahmad, Z., Holben, B. N., Smirnov, A., et al.: SeaWiFS Ocean Aerosol Retrieval (SOAR): Algorithm, validation, and comparison with other data sets. J. Geophys. Res. Atmos., **117**(D3), D03206. doi.org/10.1029/2011JD016599, 2012,

Sayer, A. M., Hsu, N. C., Lee, J., Carletta, N., Chen, S.-H., and Smirnov, A.: Evaluation of NASA Deep Blue/SOAR aerosol retrieval algorithms applied to AVHRR measurements, J. Geophys. Res. Atmos., 122, doi:10.1002/2017JD026934, 2017.

Sayer, A. M., Hsu, N. C., Lee, J., Bettenhausen, C., Kim, W. V., & Smirnov, A..: Satellite Ocean Aerosol Retrieval (SOAR) algorithm extension to S-NPP VIIRS as part of the "Deep Blue" aerosol project. J. Geophys. Res. Atmos. 123(1), 380-400, 2018.

Tanré, D., Kaufman, Y. J., Herman, M., and Mattoo, S.: Remote sensing of aerosol properties over oceans using the MODIS/EOS spectral radiances, J. Geophys. Res., 102(D14), 16971-16988, doi: https://doi.org/10.1029/96JD03437, 1997.

Torres, O., Bhartia, P. K., Herman, J. R., Ahmad, Z., and Gleason, J.: Derivation of aerosol properties from satellite measurements of backscattered ultraviolet radiation: Theoretical basis, J. Geophys. Res., 103(D14), 17099–17110, doi: https://doi.org/10.1029/98JD00900, 1998.

Torres, O., Bhartia, P. K., Herman, J. R., Syniuk, A., Ginoux, P., and Holben, B.: A long term record of aerosol optical depth from TOMS observations and comparison to AERONET measurements, J. Atmos. Sci., 59, 398– 413, doi: https://doi.org/10.1175/1520-0469(2002)059<0398:ALTROA>2.0.CO;2, 2002.

Torres, O., Tanskanen, A., Veihelmann, B., Ahn, C., Braak, R., Bhartia, P. K., Veefkind, P., and Levelt, P.: Aerosols and surface UV products from Ozone Monitoring Instrument observations: An overview, J. Geophys. Res., 112, D24S47, doi: https://doi.org/10.1029/2007JD008809, 2007.

Torres, O., Bhartia, P. K., Jethva, H., and Ahn, C.: Impact of the ozone monitoring instrument row anomaly on the long-term record of aerosol products, Atmos. Meas. Tech., 11, 2701–2715, https://doi.org/10.5194/amt-11-2701-2018, 2018.

Torres, O., Jethva, H., Ahn, C., Jaross, G., and Loyola, D. G.: TROPOMI aerosol products: evaluation and observations of synoptic-scale carbonaceous aerosol plumes during 2018–2020, Atmos. Meas. Tech., 13, 6789–6806, https://doi.org/10.5194/amt-13-6789-2020, 2020a.

Torres, O., Bhartia, P.K., Taha, G., Jethva, H., Das, S., Colarco, P., et al: Stratospheric injection of massive smoke plume from Canadian boreal fires in 2017 as seen by DSCOVR-EPIC, CALIOP, and OMPS-LP observations. J. Geophys. Res. Atmos., 125, e2020JD032579. https://doi.org/10.1029/2020JD032579, 2020b.

Tucker, C. J.: Red and photographic infrared linear combinations for monitoring vegetation. Remote Sensing of Environment, 8(2),127–150, doi.org/10.1016/0034-4257(79)90013-0, 1979.

Wagner, R., Ajtai, T., Kandler, K., Lieke, K., Linke, C., Müller, T., Schnaiter, M., and Vragel, M.: Complex refractive indices of Saharan dust samples at visible and NUV wavelengths: a laboratory study, Atmos. Chem. Phys., 12, 2491–2512, doi: https://doi.org/10.5194/acp-12-2491-2012, 2012.

Zhou, Y., Levy, R. C., Remer, L. A., Mattoo, S., & Espinosa, W. R.: Dust aerosol retrieval over the oceans with the MODIS/VIIRS dark target algorithm: 2. Nonspherical dust model. Earth and Space Science, 7, e2020EA001222, doi: https://doi.org/10.1029/2020EA001222, 2020b.

Zhou, Y., Levy, R. C., Remer, L. A., Mattoo, S., Shi, Y., & Wang, C: Dust aerosol retrieval over the oceans with the MODIS/VIIRS Dark-Target algorithm: 1. Dust detection, Earth and Space Science, 7, e2020EA001221, doi: https://doi.org/10.1029/2020EA001221, 2020a.